AIAA SciTech Forum
23-27 January 2023, National Harbor, MD & Online
AIAA SCITECH 2023 Forum
10.2514/6.2023-0243

Low Speed Characteristics Study of Various Supersonic Airfoils Using Co-Flow Jet Active Flow Control

Zhijin Lei * Gecheng Zha †
Dept. of Mechanical and Aerospace Engineering
University of Miami, Coral Gables, Florida 33124

Abstract

This paper studies the lift enhancement effect of Co-Flow Jet (CFJ) at takeoff condition for three thin airfoils at free-stream Mach numbers of 0.1, 0.2 and 0.3. Parametric studies are conducted to investigate the effect of the jet momentum coefficients (C_μ), angles of attack (AoA), flap deflection angles(δ), camber, maximum thickness, and influence of freestream Mach number to three 2-D CFJ supersonic airfoils. The simulations employ a 2-D RANS solver with Spalart-Allmaras (S-A) turbulence model, 5th order WENO scheme for the inviscid fluxes and 2nd order central differencing scheme for the viscous terms.

Numerical simulation shows that, for both unflapped and flapped 2-D CFJ supersonic airfoils, camber plays much more important role than thickness in lift enhancing. With the same maximum thickness of 4%, a cambered unflapped CFJ airfoil can increase C_L by 89% compared to a symmetric one, while with the same maximum thickness increases for 33.3% almost no lift increment is observed on a 3% symmetric unflapped CFJ airfoil. When there is a 20%c plain flap deflected for 45°, a 4% cambered CFJ airfoil can still increase C_L by around 40% compared to a symmetric one with same maximum thickness. Meanwhile, the injection flow near the leading edge can limit the extra separation around the region caused by a pointed geometric shape, which provides great potential to combine CFJ application to an optimized modern supersonic wing profile. The study also shows that, with the maximum thickness of 4%, the turning design of current CFJ ducts are all effective in the Mach number range of 0.1-0.3 at a low C_μ of 0.08, which adds confidence of its realistic availability during actual takeoff and landing.

Nomenclature

CFJ	Co-flow Jet
SST	Supersonic Civil Transport
AoA	Angle of Attack
C_L	Lift Coefficient $L/(q_\infty S)$
C_D	Drag Coefficient $D/(q_\infty S)$
C_μ	Jet Momentum Coefficient $\dot{m}_j U_j/(q_\infty S)$
$C_L/C_{D,c}$	CFJ Airfoil Corrected Lift-Drag Ratio $L/(q_\infty S U_\infty)$
LE	Leading Edge
M_∞	Freestream Mach Number
P	Pumping Power

* Graduate Student
† Professor, ASME Fellow, AIAA associate Fellow

SST	Suction Surface Transportation
S_{wing}	Wing Area
$S_{Takeoff}$	Takeoff Distance
TE	Trailing Edge
U	Flow Velocity
V_1	Decision Speed, the maximum speed at which a rejected takeoff can be initiated in the event of an emergency;
$\dot{m}$	Mass Flow
c	Chord Length
p_t	Mass-averaged Static Pressure
q	Dynamic Pressure $0.5\,\rho U^2$
α	Angle of Incidence
δ	Flap deflection Angle
γ	Specific Heat Ratio
η	Pump Efficiency
ρ	Air Density
∞	Free Stream Conditions
$_j$	Jet Conditions

1 Introduction

1.1 Backgrounds and State of the Art Overview

Supersonic Civil Transports (SST) remain a strong interest in the aviation research community and industry. High efficiency and low sonic boom are crucial for the SST's economic viability. The higher the cruise speed, the more difficult to meet the stringent requirements of low speed, which determines the community noise and runway length. The challenge for supersonic aircraft at low speed is to achieve a high lift coefficient, which is more difficult to obtain because the wing is highly swept and is formed by using thin airfoil with a small wing area.

The state-of-the-art SST low-speed performance is not encouraging. The standard landing of Tu-144 requires a drogue parachute. As shown in Table 1, Concorde normally takes about 12,000 ft to take off, which almost exceeds the length of the longest runway of the John F. Kennedy International Airport. To reduce the required runway length of supersonic civil transports, NASA requires in its SST N+2 Program that the design of 30-passenger supersonic business jets and 100-passenger commercial jets must limit their takeoff runway requirements within 10,000 ft, and expect them to be less than 9,000 fts[1].

Table 1: C_{Lmax}, S_{wing}, $S_{Takeoff}$ and Takeoff Velocity of Existing SSTs, compared with B767-200ER.

Aircraft	Weight, lb	C_{Lmax}	S_{wing}, ft^2	$S_{Takeoff}$, ft	Takeoff Velocity, mph
Tu-144LL[2, 3]	455,950	0.612	5,450	9,613	220
Concorde[4]	400,000	0.77	3,856	11,800	250
B767-200ER[5]	395,000	$\simeq 2$	3,050	8,150	140-190

Table 1 shows the maximum takeoff lift coefficient, wing area and required takeoff runway length of Concorde, Tu-144LL and B767-200ER(as comparison). It can be indicated that, if the lift coefficient of SST during takeoff can be drastically ameliorated, the takeoff runway requirement, possibly as well as the wing area and other configuration design factors, could be tremendously improved.

Lei *et al* investigated potentials of CFJ-application on 2-D symmetric thin airfoils[8], achieves a 21.6% C_L increase as well as a 14.6% $C_L/C_{D,c}$ increase at AoA=7° without flap, and a 42.5% C_L increase at α=0° with a lowered plain flap with deflection angle of 45°. When a pair of canard or horizontal tail is added to fuselage, it's possible to apply a plain flap to a supersonic wing[9]. However, due to the momentum balancing issue introduced by popular tailless-delta-wing configuration, the wings of most supersonic civil transports, such as Concorde, do not have a lowered flap during takeoff and landing[10]. The CFJ performance on unflapped wings should be further investigated. Moreover, Modern optimized supersonic wing profiles can be non-symmetric[11, 10]. This leads to interests in studying of the influence of camber on CFJ-Supersonic-Airfoils.

Realistic supersonic wings usually have a pointed leading edge to reduce shock drag during supersonic cruising. For example, the wing of Lockheed F-104 Starfighter has a leading edge radius of 0.0016 inch[12]. Whether and how this characteristics will influence the lift enhancement effect brought by CFJ, where a injection slot is located near LE, needs to be investigated.

In the previous supersonic airfoil study[8], only one free stream Mach number of 0.1 is investigated. However, the takeoff speed of Concorde is 250mph or 0.337 Mach, while the decision speed (V_1) is 150 knots or 0.232 Mach[4]. For a CFJ-boosted supersonic wing, it's crucial to ensure that the CFJ suct system is always theoretically functional during this speed range, and does not cause sudden lift loss as aircraft accelerates.

1.2 Co-Flow Jet (CFJ) Active Flow Control

The CFJ developed by Zha *et al*[13, 14, 15, 16, 17, 18, 19, 20, 21, 22, 23, 24] is demonstrated to achieve radical lift augmentation, stall margin increase, drag reduction and moderate nose-down moment for stationary and pitching airfoils.

In a CFJ airfoil, an injection slot near the leading edge (LE) and a suction slot near the trailing edge (TE) on the airfoil suction surface are created. As shown in Fig. 1, a small amount of mass flow is drawn into the suction duct, pressurized and energized by the micro compressor, and then injected near the LE tangentially to the main flow via an injection duct. The whole process does not add any mass flow to the system and hence is a zero-net-mass-flux(ZNMF) flow control.

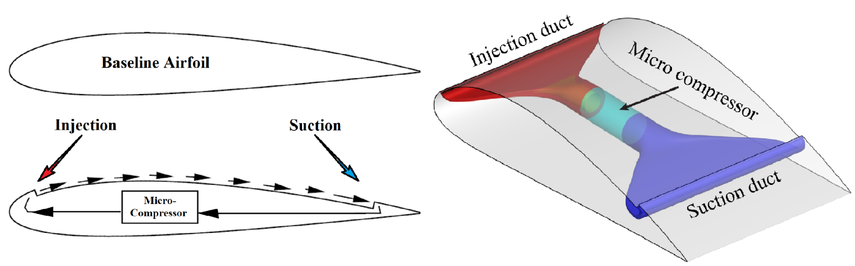

Figure 1: Schematic plot of a typical CFJ airfoil.

The jet momentum coefficient C_μ is a parameter used to quantify the jet intensity. It is defined as:

$$C_\mu = \frac{\dot{m}U_j}{\frac{1}{2}\rho_\infty {U_\infty}^2 S} \tag{1}$$

where $\dot{m}$ is the injection mass flow, U_j is the mass-averaged injection velocity, ρ_∞ and U_∞ denote the free stream density and velocity, and S is the planform area.

CFJ is implemented by mounting a pumping system inside the wing that withdraws air from the suction slot and blows it into the injection slot. The power consumption is determined by the jet mass flow and total enthalpy change as the following:

$$P = \dot{m}(H_{t1} - H_{t2}) \tag{2}$$

where H_{t1} and H_{t2} are the mass-averaged total enthalpy in the injection cavity and suction cavity respectively, P is the Power required by the pump and $\dot{m}$ the jet mass flow rate.

Introducing P_{t1} and P_{t2} the mass-averaged total pressure in the injection and suction cavity respectively, the pump efficiency η, and the total pressure ratio of the pump $\Gamma = \frac{P_{t1}}{P_{t2}}$, the power consumption is expressed as:

$$P = \frac{\dot{m} C_p T_{t2}}{\eta}(\Gamma^{\frac{\gamma-1}{\gamma}} - 1) \tag{3}$$

where γ is the specific heat ratio equal to 1.4 for air, the power coefficient is expressed as:

$$P_c = \frac{P}{\frac{1}{2}\rho_\infty U_\infty^3 S} \tag{4}$$

for a CFJ wing that has a corrected aerodynamic efficiency of

$$(\frac{L}{D})_c = \frac{C_L}{C_D + P_c.} \tag{5}$$

The current studies on CFJ are mainly focuses on thick wings and airfoils. Lei *et al* discussed theoretical possibility of applying CFJ to thin airfoil to improve the takeoff / landing performance of supersonic civil transports[8] and numerically applied it to a particular delta wing[25]. This paper will further study 2-D thin CFJ-airfoils with varied shapes and under more complicated flow conditions.

2 Numerical Simulations Overview

2.1 CFD Code

An in-house CFD code FASIP (Flow-Acoustics-Structure Interaction Package) is used to conduct all the numerical simulations. The 2-D Reynolds-Averaged Navier-Stokes (RANS) equation is used with one-equation Spalart-Allmaras turbulence model. A 5th order WENO scheme for the inviscid flux and a 2nd order central differencing for the viscous terms are employed to discretize the Navier-Stokes equations. The low diffusion E-CUSP scheme used as the approximate Riemann solver suggested by Zha *et al*[26] is utilized with the WENO scheme to evaluate the inviscid fluxes. Implicit time marching method using Gauss-Seidel line relaxation is used to achieve a fast convergence rate [27]. Parallel computing is implemented to save wall-clock simulation time. The RANS solver is validated for CFJ static airfoil simulation[28].

2.2 Baseline Models and Meshes

Three baseline airfoils are used in this study. To further imitate the characteristics of a typical supersonic wing profile, two other thin symmetric airfoils based on ONERA Wing D-Section profile, referred as M64P(maximum thickness 4.0%), and M63P(maximum thickness 3.0%), are generated and studied. The methodology of generating M64P and M63P are described as airfoil OD3P in [8]. Meanwhile, a thin airfoil from HS-1 family[29] designed for high-speed propeller, HAM-STD-1-404, which has a maximum thickness of 4.0% at 18% chord length and maximum camber 3.1% at 46% chord length, is also used as a baseline to simulate supersonic wing profiles. The shapes of all three baseline geometries are shown in Fig. 2.

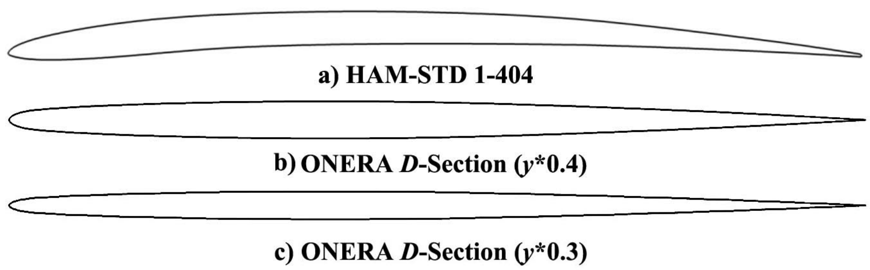

Figure 2: Baseline geometry.

The CFD meshes are constructed using the O-mesh topology in order to achieve high quality around the airfoil. Each total baseline mesh has a size of 42,000 cells with 560 points around the airfoil and 75 points normal to the airfoil. The O-mesh is split into 14 blocks for the parallel computing. To resolve the turbulent flow near wall boundary, the boundary layer spacing is defined to have $y_+ = 0.5$ at M_∞=0.1, and $y_+ = 1.0$ at M_∞=0.2. When M_∞ is increased to 0.3, y_+ will become 1.5.

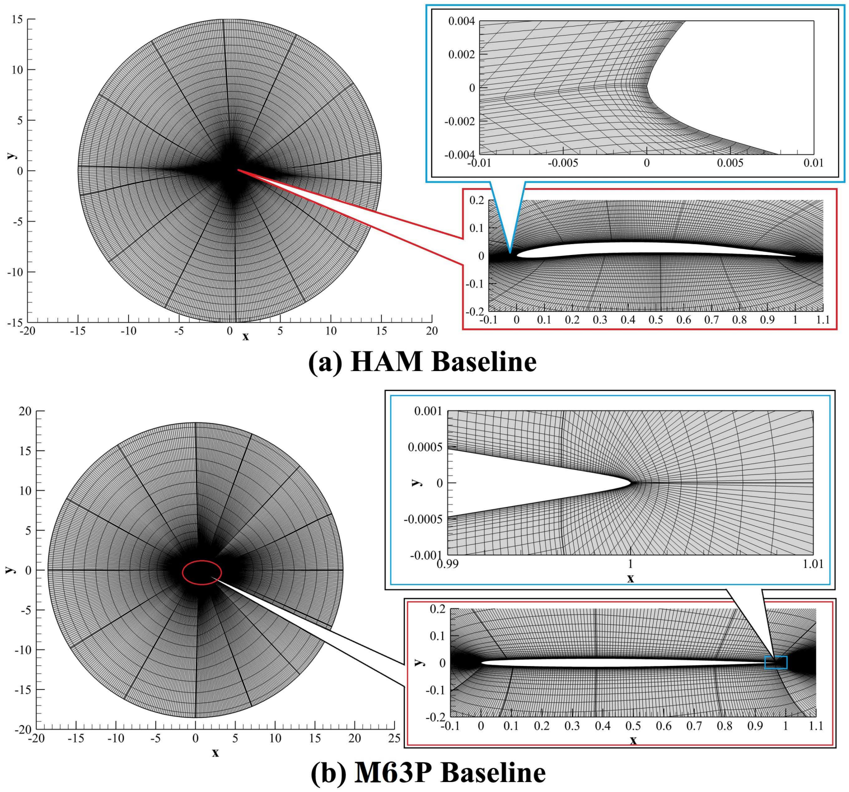

Figure 3: Two baseline meshes.

To conduct a mesh-dependence analysis, two refined meshes for each geometry are generated with the cell amount shown in Table 2, where the first one is refined with 100% more cells in radial direction and $y_+ = 0.25$, while another is refined with 100% more cells in streamwise direction along the airfoil. The converged lift and drag coefficient results at at M_∞=0.1, Re=2.85×10^6 and AoA=4° are shown in Table 2. It can be concluded that, the 560 × 75 mesh is capable enough for baseline study of all three airfoils at the major-focused M_∞ of 0.1.

Table 2: Lift and Drag Comparison of Three Airfoils at M=0.1, Re=2.85×10^6. AoA=4°.

Data	C_L	C_D
HAM-Baseline, Mesh Size of 560 × 75	0.5430	0.0108
HAM-Baseline, Mesh Size of 560 × 150	0.5461	0.0105
HAM-Baseline, Mesh Size of 1120 × 75	0.5448	0.0107
M64P-Baseline, Mesh Size of 560 × 75	0.2996	0.0073
M64P-Baseline, Mesh Size of 560 × 150	0.2998	0.0071
M64P-Baseline, Mesh Size of 1120 × 75	0.2994	0.0071
M63P-Baseline, Mesh Size of 150 × 60	0.4156	0.0102
M63P-Baseline, Mesh Size of 560 × 75	0.2977	0.0073
M63P-Baseline, Mesh Size of 560 × 150	0.2984	0.0072
M63P-Baseline, Mesh Size of 1120 × 75	0.2983	0.0071

The coefficient of lift and drag versus varied AoA are shown in Figure 4. Considering the good acceptance, the baseline meshes with cell amount of 560 × 75 are adopted for all following studies in this paper.

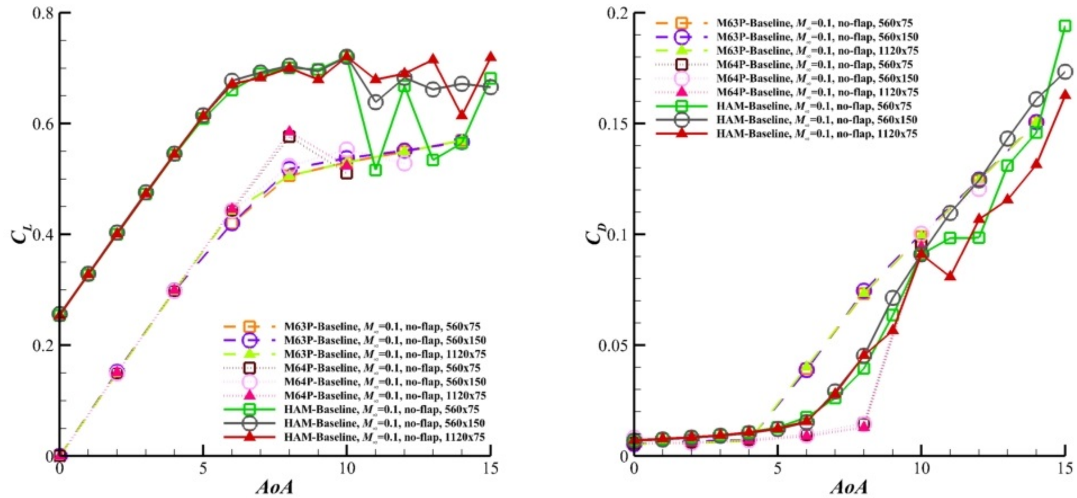

(a) Lift Coefficient (b) Drag Coefficient

Figure 4: C_L, C_D Mesh-independence validation results.

2.3 CFJ Models and Boundary Conditions

A theoretical methodology of applying CFJ sets to a lowered plain flap are numerically simulated in [8] referred as CFJ-2, where a good performance is achieved. However, the aft regions of flaps are too thin to contain a turned duct that can recycle flow collected by the suction slot. In this study, only the more-realistic CFJ-1 style configurations are further investigated, where CFJ injection slot is located near leading edge and suction slot is located before the supposed flap hinge.

An optimal CFJ location study is conducted, and three optimized CFJ designs on each baseline airfoil are selected and sketched in Fig. 5. In CFJ-HAM geometry, the injection slot is located at 0.9% chord length and has a width of $0.35\%c$, while the suction slot is located at $74.6\%c$ with a width of $1.05\%c$. In both M6-series geometries, the injection slots are located at $0.74\%c$ with a width of 9% of maximum thickness($0.27\%c$ for M63P and $0.36\%c$ for M64P), while the suction slot is located at $76.2\%c$ and has a width of 33% of maximum thickness($0.99\%c$ for M63P and $1.32\%c$ for M64P). The suction slot width and orientation are designed based on the conclusion of best performing configuration of Liu *et al*[30]. For CFJ wings and airfoils, a Suction Surface Translation (SST) is defined by translating suction surface (upper surface) slightly downward to make the tangential injection jet more smooth. However, in this thin-airfoil study, a meaningful SST significantly reduces thickness, which can be critical in producing lift. Thus, an SST of zero is adopted in all CFJ airfoils.

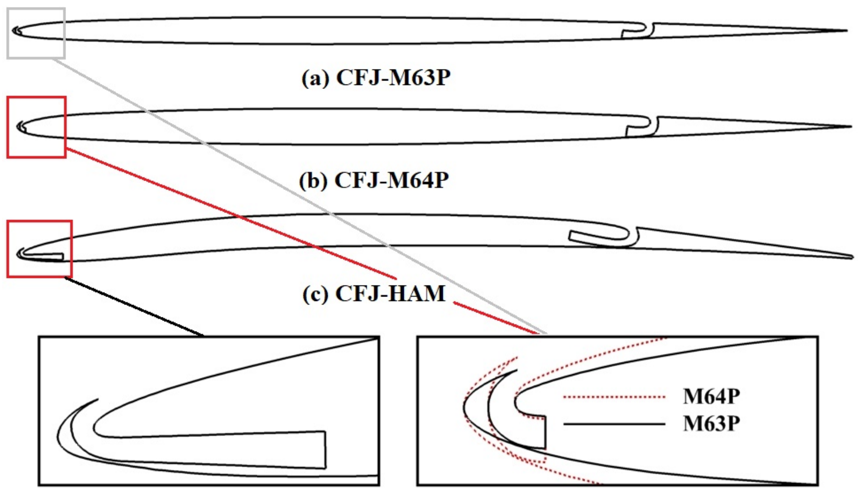

Figure 5: Schematics of basic CFJ airfoils, without lowered flaps nor pointed leading edges.

In the CFJ numerical simulation, the wall treatment suggested in [31] to achieve the 3rd order accuracy is employed. Total pressure, total temperature and flow angle are specified as the inlet boundary conditions for the upstream side of the far-field boundary and inside the injection cavity. Constant static pressure is used downstream at the far-field boundary and in the suction cavity.

To achieve zero-net mass-flux with the CFJ flow control, the injection mass flow must be equal to the mass flow entering the suction slot. Additionally, the jet strength must be controlled in order to reach the prescribed C_μ. This is achieved by iterating the jet total pressure until the C_μ value is within 1% of the prescribed value. At the suction, the suction mass flow is matched to the injection mass flow by iterating the static pressure at the suction cavity. The process is iterated throughout the simulation until the specified momentum coefficient is achieved and the injection and suction mass flow match.

3 Results and Discussion

3.1 General Characteristics: Influence of Camber and Thickness

Numerical simulation is performed on Baseline- and CFJ-airfoil of all three types mentioned above at $M_\infty = 0.1$, Re = 2,852,740. Flow field and pressure distribution of CFJ-HAM airfoil with C_μ=0.08 at AoA=0° are depicted in Fig. 6.

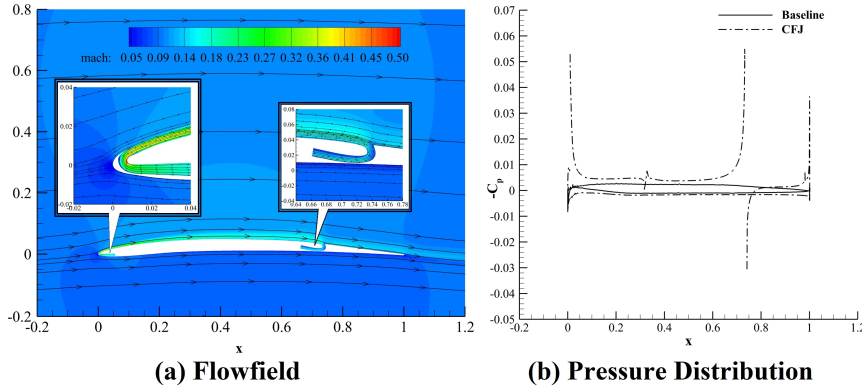

Figure 6: Flow field contoured by Mach number and pressure distribution around CFJ-HAM airfoil at M_∞ = 0.1, Re = 2,852,740, C_μ=0.08.

The flow fields around symmetric Baseline- and CFJ-M63P airfoil with a fixed C_μ of 0.5 at AoA=6° are shown in Fig. 7(d) and (e). It can be seen that, at large AoAs, the high-speed jet over the suction surface fully removed the flow separation. Fig. 7 (a), (b) and (c) compares the Mach contours of the baseline airfoil at AoA=6°, CFJ airfoil at AoA=12° and CFJ airfoil at AoA=15°. It can be clearly seen that the baseline is already massively separated at AoA=6°, whereas the CFJ airfoil remain well attached at AoA of 15°, or CFJ significantly delayed the stall of this airfoil.

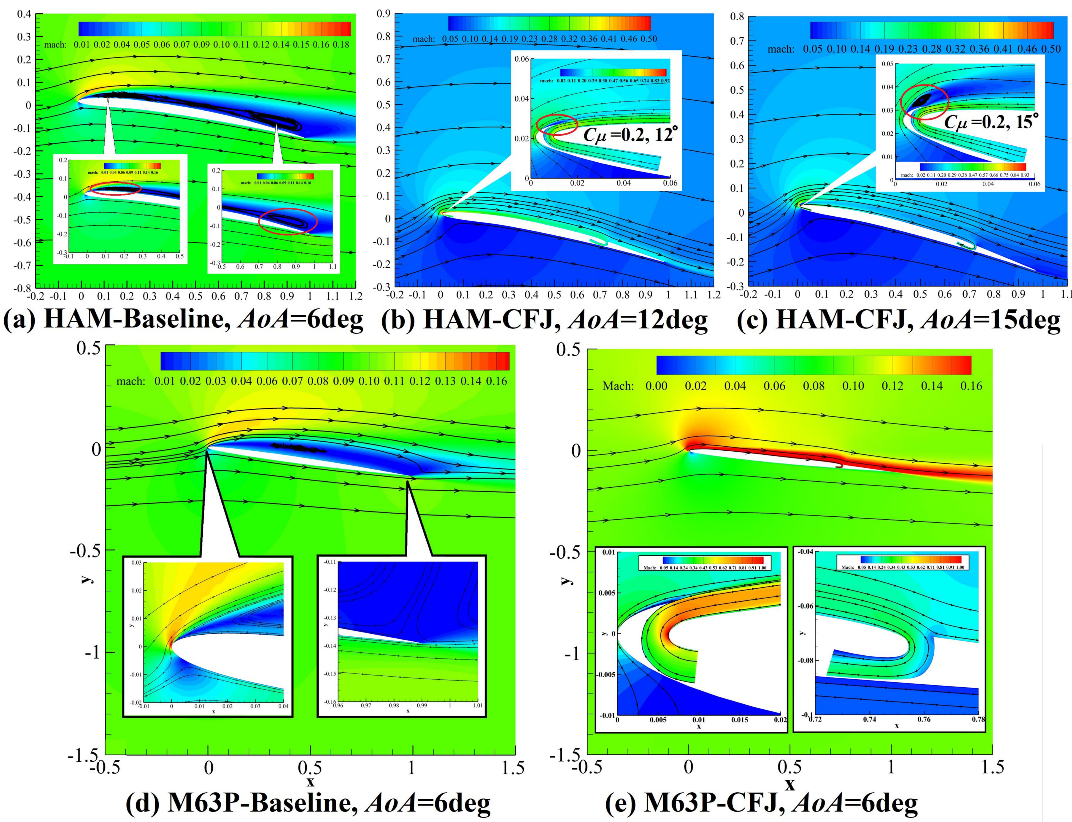

Figure 7: Mach number contours around the baseline and CFJ airfoils at M_∞ = 0.1, Re = 2,852,740, with varied AoAs and C_μs.

When AoA further increases, the suction flow separation can be still suppressed by providing a larger C_μ, especially for symmetric airfoils. However, due to the limited space for injection and suction ducts, a C_μ that is too large may easily lead to a choked injection slot as well as suction slot, as shown in Fig. 8.

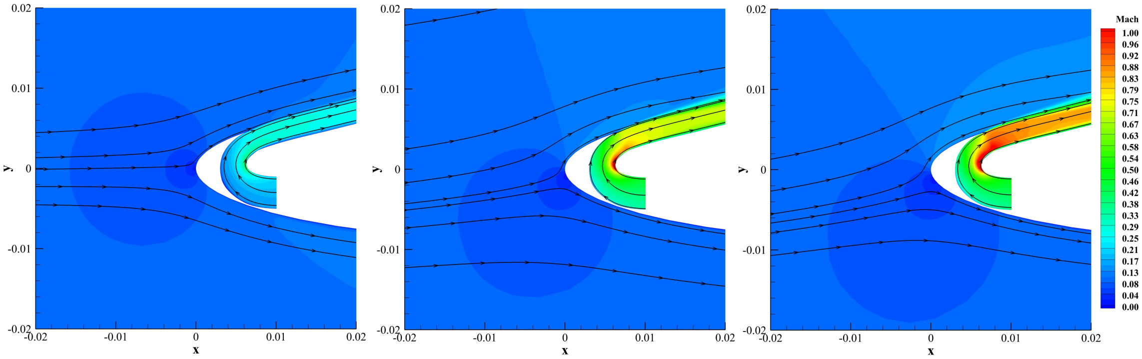

(a) C_μ =0.08 (b) C_μ =0.3 (c) C_μ =0.4

Figure 8: Injection region flow field evolution when C_μ increases from 0.08 (a) to 0.4 (c).

To investigate the influence of this phenomenon, the Mach contours of CFJ-HAM airfoil at a critical AoA of 15° with increased C_μs are shown in Fig. 9(a) with a C_μ of 0.4, where the injection flow is about to reach supersonic. When C_μ approaches 0.5 and 0.6 as Fig. 9(b) and (c) displays, the injection is fully choked, while the suction slot still functions well, and the overall flow is well attached.

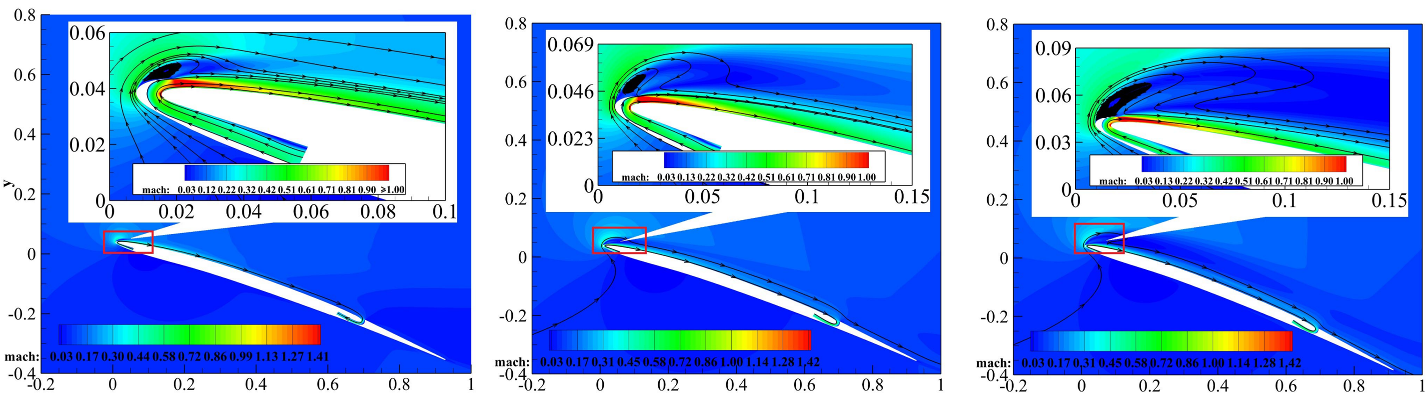

(a) C_μ=0.4 (b) C_μ=0.5 (c) C_μ=0.6

Figure 9: Evolution of LE separation bubble when C_μ is increased. $M_\infty = 0.1$, Re = 2,852,740, AoA=15°.

To study the influence of thickness and camber to CFJ-airfoil performance, the lift coefficient of CFJ-HAM, CFJ-M64P and CFJ-M63P versus baseline at $AoA = 4°$ are compared in Table 3.

During takeoff and landing, which is a time-transient process, the most important aerodynamic performance is lift instead of (corrected) lift / drag ratio. The lift coefficient of CFJ-HAM, CFJ-M64P and CFJ-M63P with two C_μs versus AoA are compared in Fig. 10.

Table 3: CFJ C_L Comparison, $AoA = 4°$, $M_\infty = 0.1$, Re = 2,852,740, no-flap.

C_μ	Type	C_L	ΔC_L from Baseline	ΔC_L from CFJ-M64P	P_c
0.08	HAM	0.709	29.3%	89.1%	0.120
0.08	M63P	0.361	21.0%	-3.7%	0.127
0.08	M64P	0.375	25.7%	-	0.112
0.5	HAM	1.066	93.8%	88.7%	2.401
0.5	M63P	0.519	73.2%	-8.1%	2.615
0.5	M64P	0.565	88.4%	-	2.551

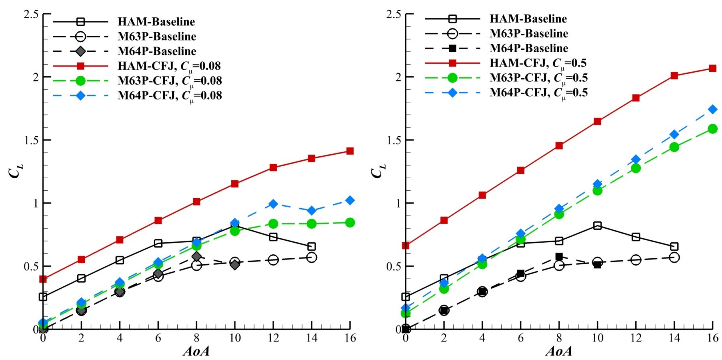

Figure 10: Lift and power coefficient with varied cambers and thicknesses, δ=0°.

The result indicates that, without the advantage of a plain flap, a properly designed camber provides much better CFJ performance when the airfoil thickness is fixed. The lift, drag, power coefficient, aerodynamic lift / drag ratio C_L/C_D and corrected lift / drag ratio C_L/C_D of the cambered CFJ-HAM airfoil versus AoA are plotted in Fig. 11. It can be inferred theoretically that, the lift / drag ratio will be declined significantly due to the introduced power coefficient. However, when C_μ is reasonably given to 0.08, the actual lift / drag ratio will become even higher than baseline when AoA is above 8°, which suggests that during this takeoff / landing process the CFJ-airfoil can still be more energy efficient than baseline.

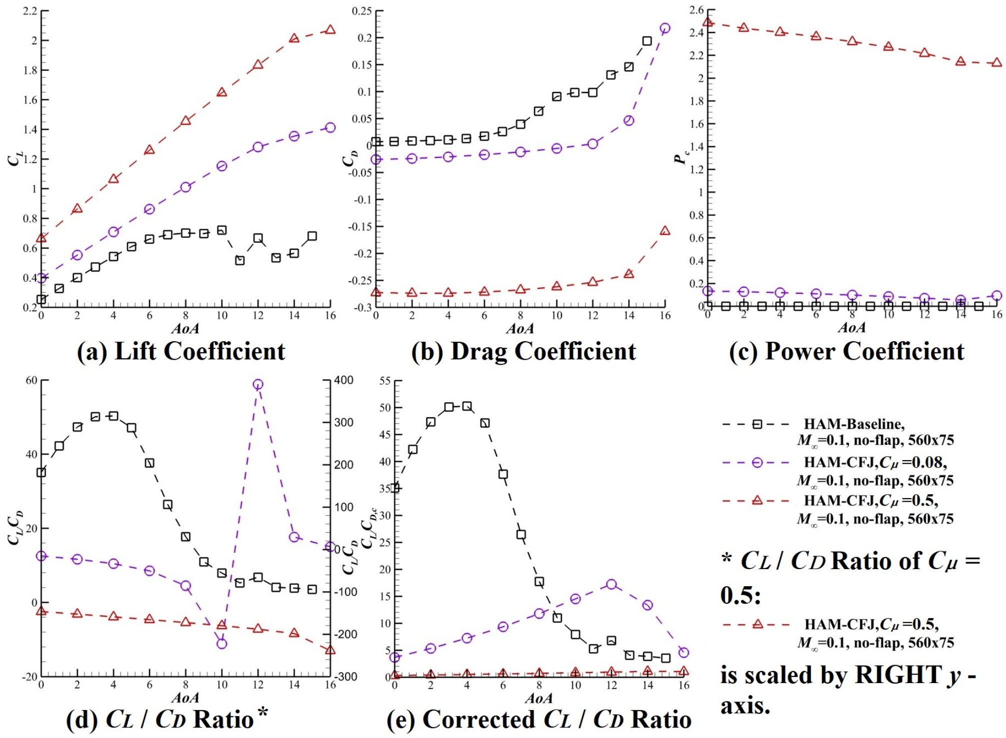

Figure 11: Coefficient of lift, CFJ power and $(L/D)_c$ vs AoA.

3.2 Leading Edge Shape Study

Note that in Fig. 7 (b) and (c), there are small separation bubbles near the leading edge(LE) of the CFJ airfoil due to its sharp turning. As mentioned in Introduction, actual optimized supersonic wing profiles usually has a more sharpened leading edge, which may deteriorate this separation. To investigate whether and how this characteristics will influence the lift enhancement effect brought by CFJ, an alternative pointed leading edge is designed for Baseline- and CFJ-HAM airfoil, as shown in Fig. 12.

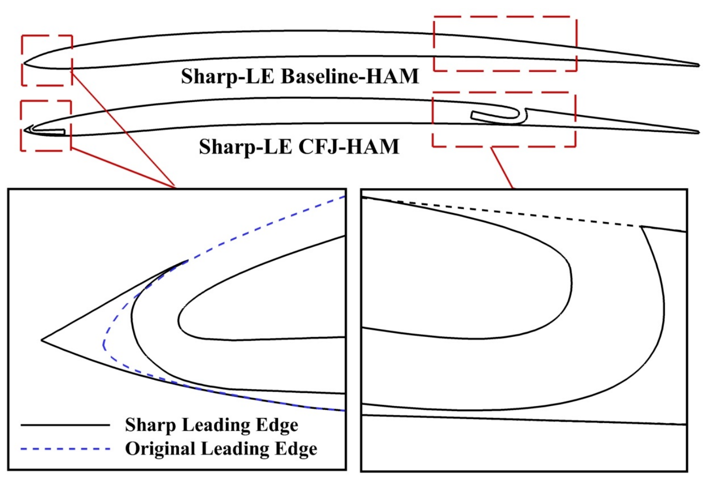

Figure 12: Schematics of pointed leading edge for both Baseline- and CFJ-airfoil.

The flow fields around original and LE-sharpened CFJ-HAM airfoils contoured by Mach number are shown in Fig. 13. It can be seen from Fig. 13(a) and (b) that, under the identical flow condition and co-flow jet intensity, the airfoil with sharp LE produces a separation near leading edge, but the scale of separation is limited by the jet flow. When the jet C_μ is increased from 0.08 to 0.5, as shown in Fig. 13(c), the leading edge separation is obviously reduced. This phenomenon is amplified at a more critical flow condition. At AoA of 14° shown in Fig. 14, while CFJ on the original airfoil is still capable to keep flow over suction surface attached, separation can be observed over the whole suction surface of LE-sharpened airfoil due to the enhanced vortices from leading edge. However, increasing C_μ can resolve this problem and attach flow over suction surface to wall boundary again, which suggests that the lift enhancement effect of CFJ will remain under this condition.

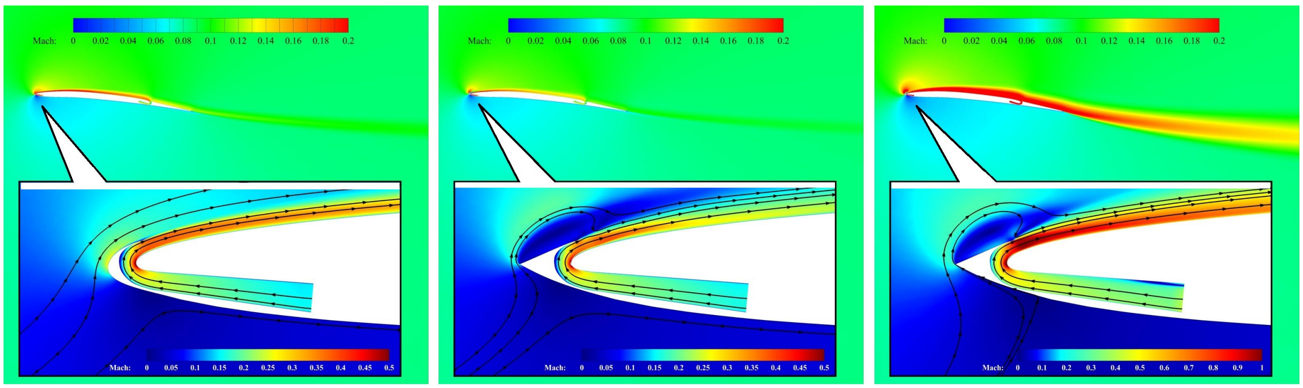

(a) Blunt LE (Original), C_μ=0.08 **(b) Sharp LE, C_μ=0.08** **(c) Sharp LE, C_μ=0.5**

Figure 13: Mach number contours around CFJ-HAM airfoils with varied LE shapes and C_μs, $M_\infty = 0.1$, $Re =$ 2,852,740, AoA=6°.

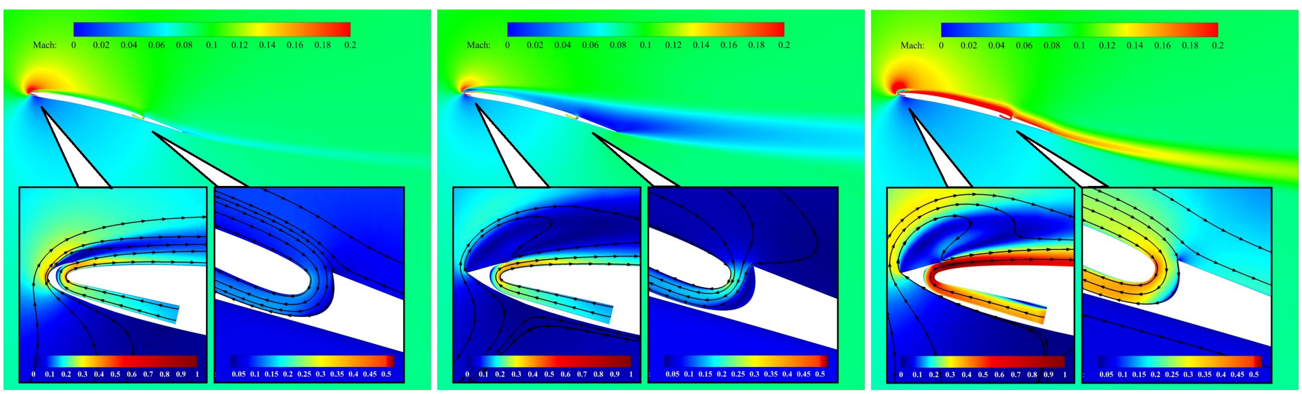

(a) Blunt LE (Original), C_μ=0.08 **(b) Sharp LE, C_μ=0.08** **(c) Sharp LE, C_μ=0.5**

Figure 14: Mach number contours around CFJ-HAM airfoils with varied LE shapes and C_μs, $M_\infty = 0.1$, $Re =$ 2,852,740, AoA=14°.

The lift coefficient, drag coefficient, power coefficient, lift / drag ratio (C_L/C_D) and corrected lift / drag ratio ($C_L/C_{D,c}$) of CFJ-HAM, CFJ-M64P and CFJ-M63P with two C_μs versus AoA are plotted in Fig. 15. The diagrams indicate that, with a small-medium C_μ such as 0.08, CFJ has almost identical aerodynamic performance on both airfoil geometries when AoA is small. As AoA increases, both lift enhancement and drag reduction effect of CFJ on the LE-sharpened airfoil are significantly weakened, and C_L/C_D drops as well as $C_L/C_{D,c}$. However, when C_μ is largely increased, this difference between two geometries is reduced due to the limitation of leading edge separation caused by strong injected jet flow.

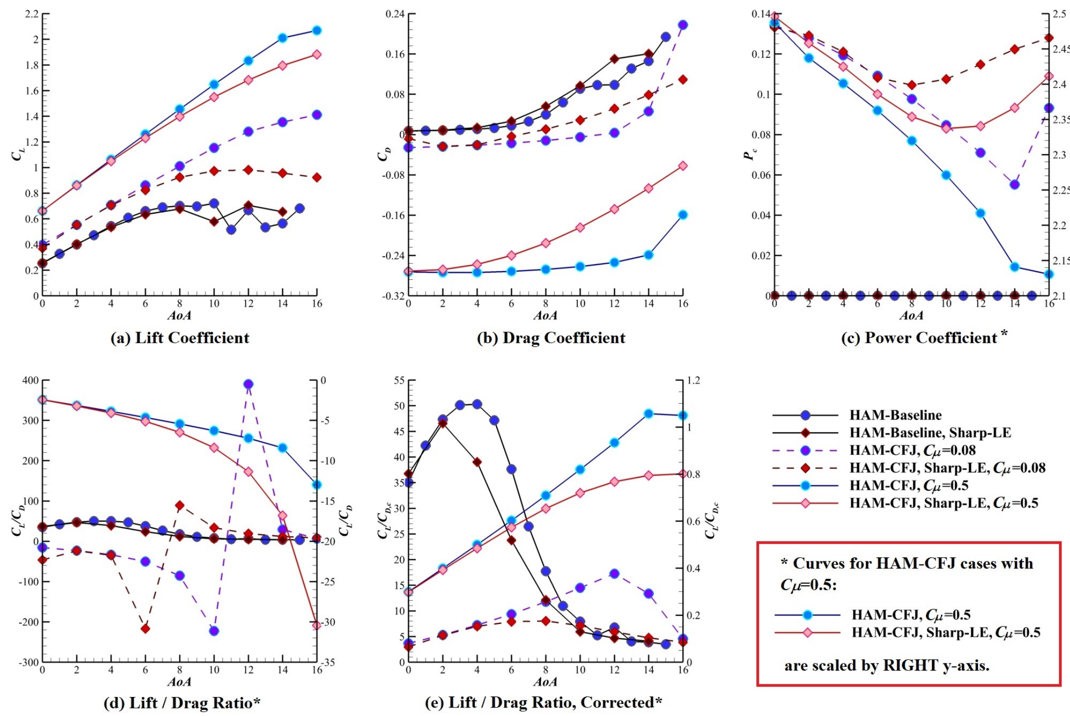

Figure 15: C_L, C_D, P_C, C_L/C_D and $C_L/C_{D,c}$ of CFJ-HAM, CFJ-M64P and CFJ-M63P with two C_μs versus AoA.

3.3 Study of Flap Influence

Flapped baseline and CFJ-mounted HAM, M63P and M64P airfoils are defined as shown in Fig. 16. Based on the initial study of [8], the optimal flap deflection angle of M63P can be equal to or larger than 45°. To further study the CFJ lift enhancement margin with a lowered flap, three large flap deflection angles δ=45°, δ=60° and δ=75° are numerically investigated.

The CFJ-HAM aerodynamic performances with varied δs with angle of incidence $\alpha = 6°$, C_μ=0.08 are compared in Table 4. With a flap deflection angle δ=45°, compared with baseline, CFJ-HAM achieves a C_L increase of 74.05%, and reduced drag by 74.36%. This leads to a 577.8% increase of C_L/C_D and a 187.8% increase of $C_L/C_{D,c}$, which tremendously improves the low-L/D problem of supersonic civil transports during takeoff and landing. Flow fields contoured by Mach number around baseline and CFJ airfoils listed in Table 4 are shown in Fig. 18. It can be inferred that, when CFJ only exists between leading edge and flap, the best flap deflection angle is 45° rather than larger.

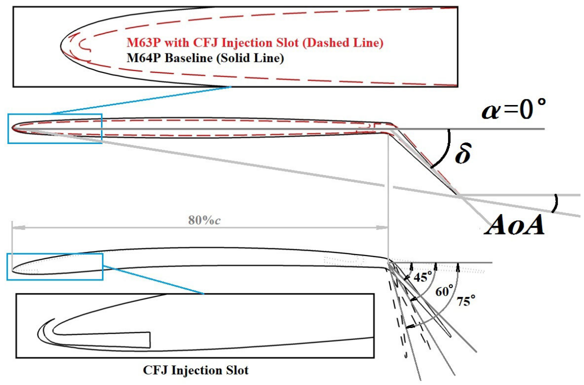

Figure 16: Schematics of flapped Baseline- and CFJ-airfoil geometries.

Table 4: Aerodynamic Performances Comparison, α = 6°, M_∞ = 0.1, Re = 2,852,740, C_μ=0.08.

CFJ δ	C_L	ΔC_L from δ=45° Baseline	C_D	C_L/C_D	$C_L/C_{D,c}$
45°	1.759	74.05%	0.049	36.070	15.179
60°	1.624	60.69%	0.079	20.500	10.835
75°	1.581	56.43%	0.122	13.017	8.275

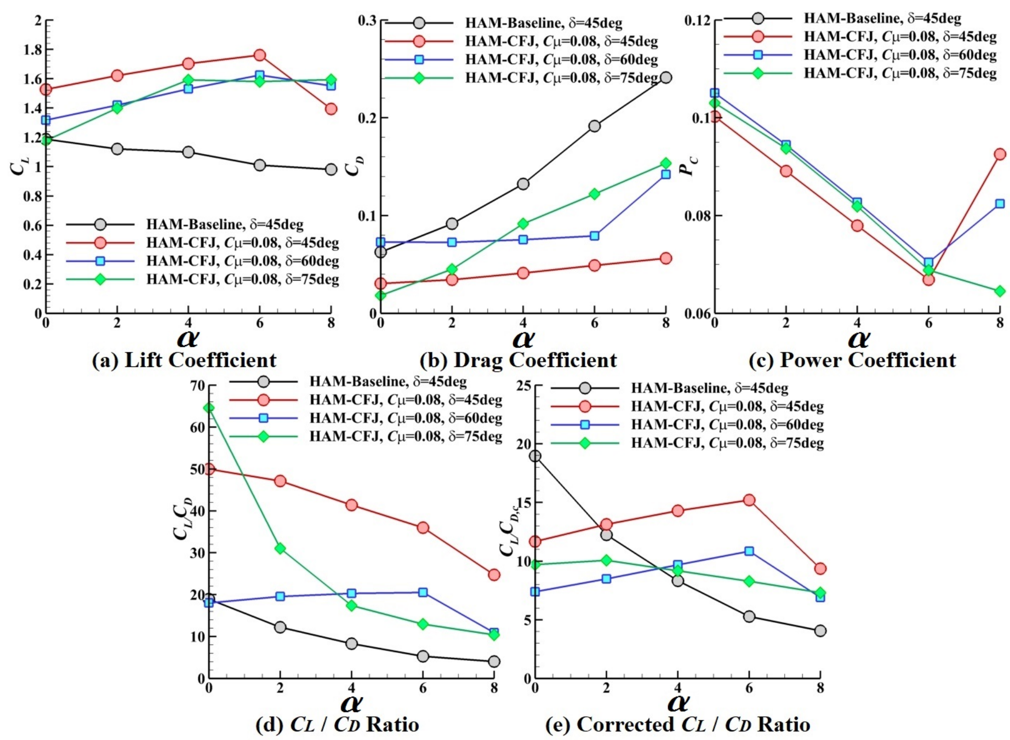

Figure 17: C_L, C_D, P_C, C_L/C_D and $C_L/C_{D,c}$ of CFJ-HAM with three varied flap deflection angles versus α. M_∞ = 0.1, Re = 2,852,740, and C_μ=0.08.

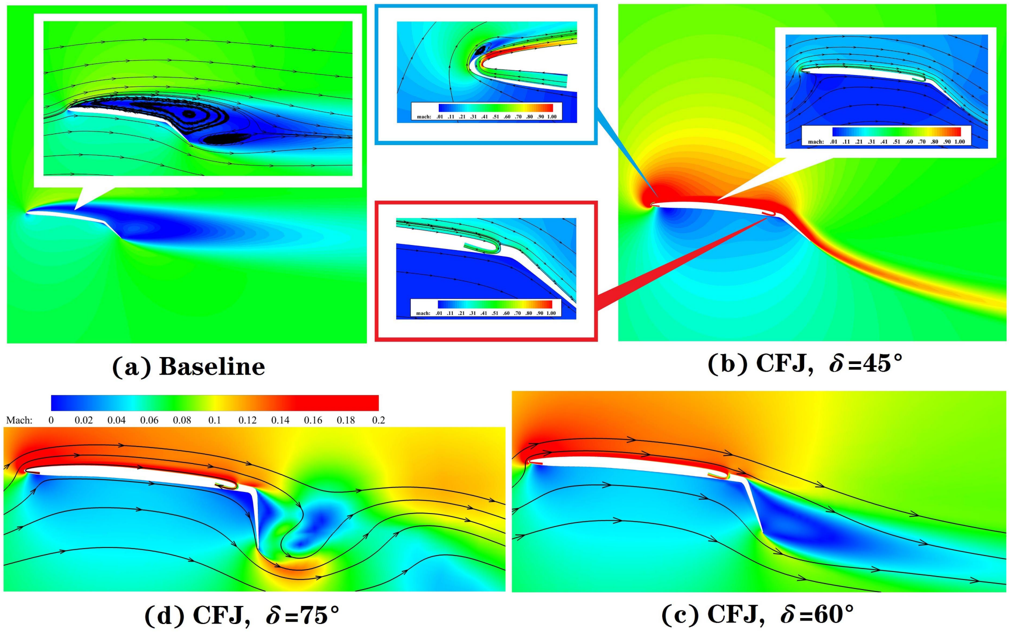

Figure 18: Mach number contour of Baseline-HAM(a) and CFJ-HAM, α=6°, CFJ C_μ=0.5, δ=45°(b), 45°(c), and 75°(d).

To investigate the influence of airfoil camber and thickness when the airfoil has an optimal deflected flap, three airfoil geometries mentioned above in Fig. 2 and Fig. 5 with the fixed flap deflection angle δ=45° are numerically simulated under the flow condition of $M_\infty = 0.1$, Re = 2,852,740. The performance results of two C_μs, namely 0.08 and 0.5, are plotted in Fig. 19(a) and (b)respectively. It can be seen that, with δ=45° at a small C_μ of 0.08, cambered airfoil still has great advantage over symmetric airfoils, while maximum thickness only makes limited difference.

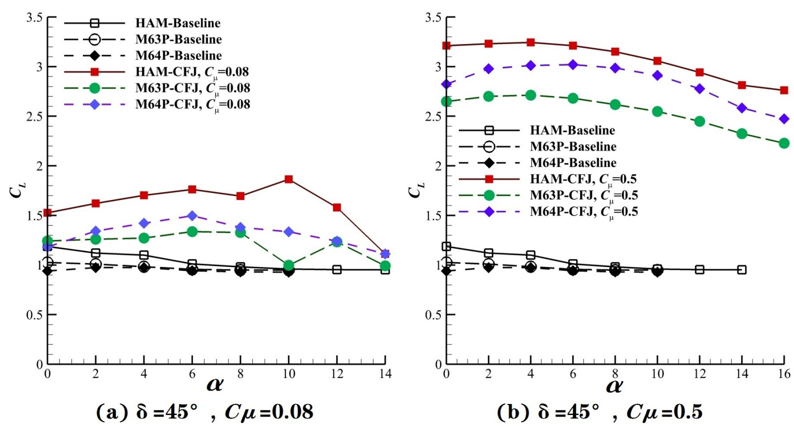

Figure 19: Lift coefficient comparison of CFJ-HAM, CFJ-M63P and CFJ-M64P with flap deflection angle δ=45° at C_μ=0.08 and C_μ=0.5, $M_\infty = 0.1$, Re = 2,852,740.

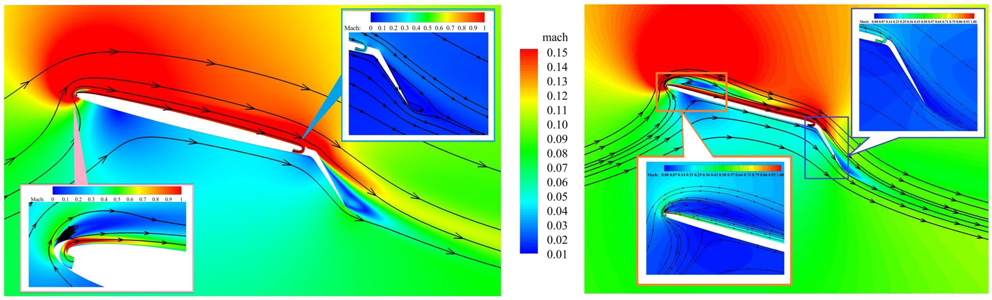

(a) M64P **(b) M63P**

Figure 20: Mach number contours of CFJ-M64P(a) and CFJ-M63P(b), α=14°, δ=45°, CFJ C_μ=0.5.

As shown in Fig. 20(b), at a large C_μ of 0.5, maximum thickness of airfoil becomes more important when CFJ is applied. The Mach contours of two CFJ airfoils with 25% maximum thickness difference and the same deflection angle of 45° are compared in Fig. 20. The flow near the injection slot of CFJ-M64P(a) is separated but in a small scale. However, in M63P, the separation is deteriorated and leads to a stable region of vortex between injected jet flow and free-stream. This weakens both lift enhancement and drag reduction performance.

3.4 Freestream Mach Number Compatibility Study

According to the definition of C_μ:

$$C_\mu = \frac{\dot{m} U_j}{\frac{1}{2}\rho_\infty {U_\infty}^2 S} \tag{6}$$

When M_∞ or U_∞ increases, to have C_μ maintained, jet flow velocity U_j must be increase as well, which can lead to CFJ duct choke due to the limited geometric size and therefore prevent actual C_μ from being increased enough to enhance airfoil lift coefficient, which is related to Three sets of free-stream takeoff accelerating conditions, namely $M_\infty = 0.1$, Re = 2,852,740; M_∞=0.2, Re = 5,705,480, and $M_\infty = 0.3$, Re = 7,242,910, are investigated to simulate this phenomenon.

Fig. 21 shows the flow field around the CFJ-HAM airfoil and near the injection as well as suction duct when the freestream Mach number increases from 0.1 to 0.3. The airfoil has an AoA of 10°, and CFJ C_μ=0.08. It can be seen that, At freestream Mach number $M_\infty = 0.1$, both injection and suction slot work normally. When M_∞ increases to 0.2, which reflects a typical determine speed ($V1$) of aircraft, the flow in injection slot is about to choke, while the flow near and inside suction slot remains normal. When M_∞ increases to 0.3, which reflects a typical takeoff speed of classic supersonic civil transports, the injection flow outside of slot is choked, and the jet flow inside suction slot is smooth but about to choke as well. This suggests that C_μ of 0.08 is the maximum possible C_μ that can be achieved and maintained by CFJ device within this speed range.

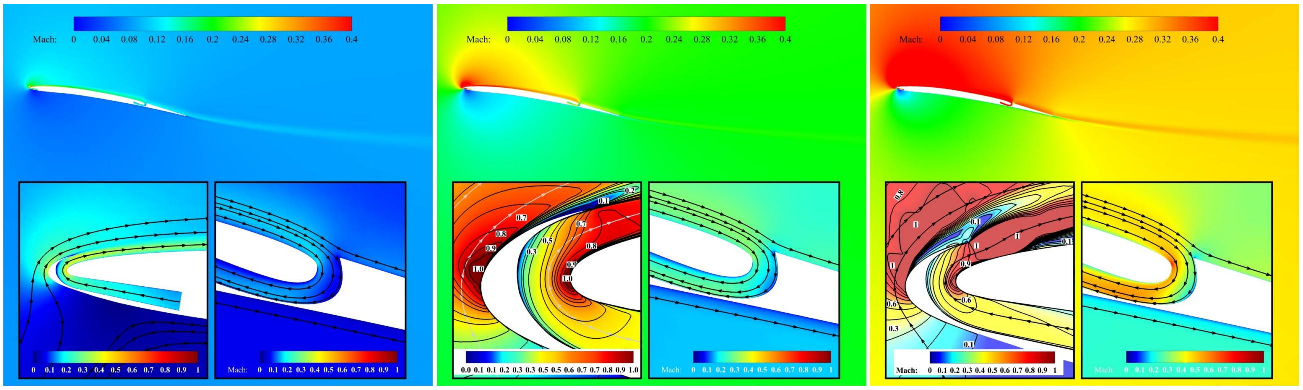

(a) C_μ=0.08, M_∞=0.1 **(b) C_μ=0.08, M_∞=0.2** **(c) C_μ=0.08, M_∞=0.3**

Figure 21: Mach number contours of unflapped CFJ-HAM at CFJ C_μ=0.08, α=10°, with varied freestream Mach number.

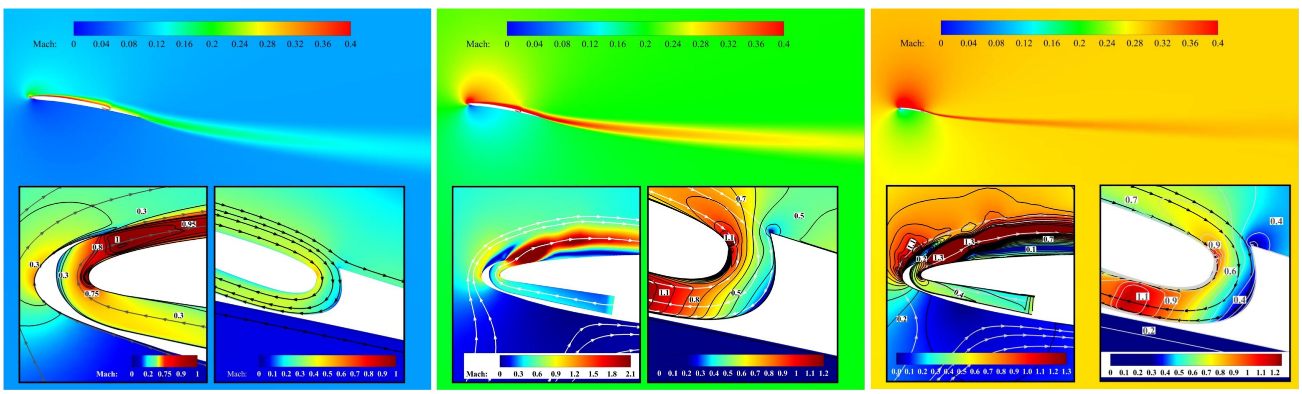

(a) C_μ=0.5, M_∞=0.1 **(b) C_μ=0.41, M_∞=0.2** **(b) C_μ=0.16, M_∞=0.3**

Figure 22: Mach number contours of unflapped CFJ-HAM with maximum possible CFJ C_μ, α=10°, with varied freestream Mach numbers.

Fig. 22 shows the flow field around the CFJ-HAM airfoil and near the injection as well as suction duct when the freestream Mach number increases from 0.1 to 0.3, but at maximum possible CFJ C_μ in every given M_∞. The airfoil still has a fixed AoA of 10°. It can be seen that, At freestream Mach number $M_\infty = 0.1$, the maximum possible C_μ is 0.5, where the injection slot is already fully choked. When M_∞ increases to 0.2, due to the choke at both injection and suction slot, the velocity of jet are capped, which leads to a reduced maximum possible C_μ of 0.41. When M_∞ increases to 0.3, the capped mass flow and velocity of jet makes the maximum possible C_μ quickly reduce to 0.16.

The influence of this duct-choke phenomenon on CFJ aerodynamic performance as M_∞ increases are numerically investigated. Comparison of baseline- and CFJ-HAM lift coefficient at three freestream Mach numbers are plotted in Fig. 23. At a fixed AoA, Non-dimensionized lift coefficient of a fixed airfoil will theoretically remain same as freestream speed increases, thus only baseline data of M_∞=0.1 is plotted. It can be seen from Fig. 23(a) that, at a fixed C_μ of 0.08 during the acceleration, CFJ lift enhancement effect increases at first (M_∞=0.2) and then slightly dropped (M_∞=0.3). However, since the injection slot is almost choked at M_∞=0.3, then power coefficient required by CFJ becomes 31.5% higher than that of M_∞=0.1 and 0.2 at AoA=0°, and becomes even higher when AoA increases, as seen in Fig. 23(b). This suggests that, as freestream speed increases, if the desired C_μ is relatively small, current CFJ-HAM design can have lift enhancement effect remained but at a much higher energy cost.

Another study is conducted to find out the maximum possible lift enhancement effect at every freestream Mach number conditions. With this strategy, the C_μ is always set to make the injection or suction slot fully choked. The lift coefficient result versus AoA is plotted in Fig. 23(c), where the maximum C_μ can be achieved at M_∞=0.1 remains 0.5, while at M_∞=0.2, it reduces to 0.41, and at M_∞=0.3 it further reduces to 0.16. However, despite this loss of extra lift enhancement potential, actual lift coefficient increase at M_∞=0.3 is still the same as that at M_∞=0.1, which means that there can be no sudden lift drop during takeoff and landing process. The current supersonic CFJ-airfoil design is safe for realistic application.

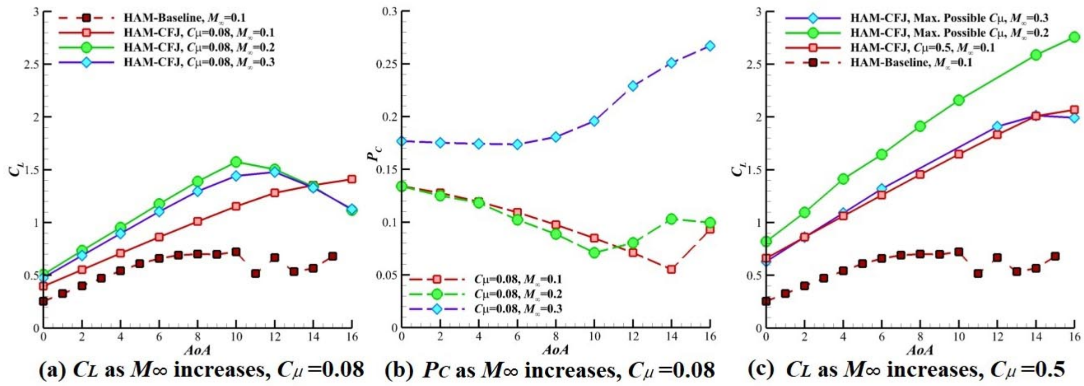

Figure 23: Comparison of C_L, C_D, P_c and $(C_L/C_D)_c$ of Baseline-HAM and CFJ-HAM airfoils at varied M_∞ and Res.

4 Conclusions

The lift enhancement effect of Co-Flow Jet (CFJ) at takeoff condition for three thin airfoils at free-stream Mach numbers of 0.1, 0.2 and 0.3 are studied. Parametric studies are conducted to investigate the effect of the jet momentum coefficients (C_μ), angles of attack (AoA), flap deflection angles(δ), camber, maximum thickness, and influence of freestream Mach number to three 2-D CFJ supersonic airfoils.

The numerical results indicate that, for both unflapped and flapped 2-D CFJ supersonic airfoils, camber plays much more important role than thickness in lift enhancing. With the same maximum thickness of 4%, a cambered unflapped CFJ airfoil can increase C_L by 89% compared to a symmetric one, while with the same maximum thickness increases for 33.3% almost no lift increment is observed on a 3% symmetric unflapped CFJ airfoil. When there is a 20%c plain flap deflected for 45°, a 4% cambered CFJ airfoil can still increase C_L by around 40% compared to a symmetric one with same maximum thickness. This conclusion suggests a great potential of improving the low speed lift performance without applying a plain flap to the wing, which is efficient but introduces control difficulties in aircraft conceptual design due to the special characteristics of the Concorde-style SSTs.

Meanwhile, the injection flow near the leading edge can limit the extra separation around the region caused by a pointed geometric shape, which provides the possibility to combine CFJ application to an optimized modern supersonic wing profile.

The study also theoretically proves that, with the maximum thickness of 4%, the turning design of the current CFJ ducts are all effective in the Mach number range of 0.1-0.3 at a low C_μ of 0.08, which adds confidence of its realistic availability during actual takeoff and landing.

5 Acknowledgment

The simulations are conducted on Pegasus super-computing system at the Center for Computational Sciences (CCS) at the University of Miami.

References

[1] H. Welge, C. Nelson, and J. Bonet, "Supersonic vehicle systems for the 2020 to 2035 timeframe," in *28th AIAA Applied Aerodynamics Conference*, p. 4930, 2010.

[2] R. E. Curry and L. R. Owens, "Ground-effect characteristics of the tu-144 supersonic transport airplane," 2003.

[3] R. A. Rivers, E. B. Jackson, C. G. Fullerton, T. H. Cox, and N. H. Princen, "A qualitative piloted evaluation of the tupolev tu-144 supersonic transport," 2000.

[4] E. Gordon, "Technical specs, http://www.concordesst.com/concordeb.html," 2001.

[5] D. A. Garvin, "Boeing 767: From concept to production (a)," 1988.

[6] D. Mavris and M. Kirby, "Takeoff / landing assessment of an hsct with pneumatic lift augmentation," in *37th Aerospace Sciences Meeting and Exhibit*, p. 534, 1998.

[7] R. L. L. Englar, "Circulation control for high lift and drag generation on stol aircraft," *Journal of Aircraft*, vol. 12, no. 5, pp. 457–463, 1975.

[8] Z. Lei and G. Zha, "Lift Enhancement of Supersonic Thin Airfoil at Low Speed by Co-Flow Jet Active Flow Control," in *AIAA AVIATION 2021 FORUM*, p. 2591, 2021.

[9] Y. Kishi, S. Kitazaki, A. Ariyarit, Y. Makino, and M. Kanazaki, "Planform dependency of optimum supersonic airfoil for wing-body-nacelle configuration using multi-fidelity design optimization," in *35th AIAA Applied Aerodynamics Conference*, p. 4468, 2017.

[10] J. Reuther, J. J. Alonso, M. J. Rimlinger, and A. Jameson, "Aerodynamic shape optimization of supersonic aircraft configurations via an adjoint formulation on distributed memory parallel computers," *Computers & fluids*, vol. 28, no. 4-5, pp. 675–700, 1999.

[11] K. Yoshida, "Supersonic drag reduction technology in the scaled supersonic experimental airplane project by jaxa," *Progress in Aerospace Sciences*, vol. 45, no. 4-5, pp. 124–146, 2009.

[12] G. J. Marrett, *Sky High in a Starfighter: My climb to the top in the F-104*. Smithsonian Magazine, 2002.

[13] G.-C. Zha and D. C. Paxton, "A Novel Flow Control Method for Airfoil Performance Enhancement Using Co-Flow Jet." *Applications of Circulation Control Technologies*, Chapter 10, p. 293-314, Vol. 214, Progress in Astronautics and Aeronautics, AIAA Book Series, Editors: Joslin, R. D. and Jones, G.S., 2006.

[14] G.-C. Zha, W. Gao, and C. Paxton, "Jet Effects on Co-Flow Jet Airfoil Performance," *AIAA Journal, No. 6,*, vol. 45, pp. 1222–1231, 2007.

[15] G.-C. Zha, C. Paxton, A. Conley, A. Wells, and B. Carroll, "Effect of Injection Slot Size on High Performance Co-Flow Jet Airfoil," *AIAA Journal of Aircraft*, vol. 43, 2006.

[16] G.-C. Zha, B. Carroll, C. Paxton, A. Conley, and A. Wells, "High Performance Airfoil with Co-Flow Jet Flow Control," *AIAA Journal*, vol. 45, 2007.

[17] Wang, B.-Y. and Haddoukessouni, B. and Levy, J. and Zha, G.-C., "Numerical Investigations of Injection Slot Size Effect on the Performance of Co-Flow Jet Airfoil," *Journal of Aircraft*, vol. Vol. 45, No. 6,, pp. pp.2084–2091, 2008.

[18] B. P. E. Dano, D. Kirk, and G.-C. Zha, "Experimental Investigation of Jet Mixing Mechanism of Co- Flow Jet Airfoil." AIAA-2010-4421, 5th AIAA Flow Control Conference, Chicago, IL, 28 Jun - 1 Jul 2010.

[19] B. P. E. Dano, G.-C. Zha, and M. Castillo, "Experimental Study of Co-Flow Jet Airfoil Performance Enhancement Using Micro Discreet Jets." AIAA Paper 2011-0941, 49th AIAA Aerospace Sciences Meeting, Orlando, FL, 4-7 January 2011.

[20] A. Lefebvre, B. Dano, W. Bartow, M. Fronzo, and G. Zha, "Performance and energy expenditure of coflow jet airfoil with variation of mach number," *Journal of Aircraft*, vol. 53, no. 6, pp. 1757–1767, 2016.

[21] A. Lefebvre, G-C. Zha, "Numerical Simulation of Pitching Airfoil Performance Enhancement Using Co-Flow Jet Flow Control," *AIAA paper 2013-2517*, June 2013.

[22] A. Lefebvre, G-C. Zha, "Cow-Flow Jet Airfoil Trade Study Part I : Energy Consumption and Aerodynamic Performance," *32nd AIAA Applied Aerodynamics Conference, AIAA AVIATION Forum, AIAA 2014-2682*, June 2014.

[23] A. Lefebvre, G-C. Zha, "Cow-Flow Jet Airfoil Trade Study Part II : Moment and Drag," *32nd AIAA Applied Aerodynamics Conference, AIAA AVIATION Forum, AIAA 2014-2683*, June 2014.

[24] Lefebvre, A. and Zha, G.-C., "Trade Study of 3D Co-Flow Jet Wing for Cruise Performance." AIAA Paper 2016-0570, AIAA SCITECH2016, AIAA Aerospace Science Meeting, San Diego, CA, 4-8 January 2016.

[25] Z. Lei and G. Zha, "Lift enhancement for highly swept 3d delta wing at low speed using coflow jet flow control," in *AIAA AVIATION 2021 FORUM*, p. 2559, 2021.

[26] Zha, G.C., Shen, Y.Q. and Wang, B.Y., "An improved low diffusion E-CUSP upwind scheme ," *Journal of Computer and Fluids*, vol. 48, pp. 214–220, Sep. 2011.

[27] G.-C. Zha and E. Bilgen, "Numerical Study of Three-Dimensional Transonic Flows Using Unfactored Upwind-Relaxation Sweeping Algorithm," *Journal of Computational Physics*, vol. 125, pp. 425–433, 1996.

[28] B.-Y. Wang and G.-C. Zha, "A General Sub-Domain Boundary Mapping Procedure For Structured Grid CFD Parallel Computation," *AIAA Journal of Aerospace Computing, Information, and Communication*, vol. 5, No.11, pp. 2084–2091, 2008.

[29] G. M. Cole, "Tapered propeller blade design," May 11 1993. US Patent 5,209,643.

[30] Z. Liu and G. Zha, "Transonic airfoil performance enhancement using co-flow jet active flow control," in *8th AIAA Flow Control Conference*, p. 3472, 2016.

[31] Y.-Q. Shen, G.-C. Zha, and B.-Y. Wang, "Improvement of Stability and Accuracy of Implicit WENO Scheme ," *AIAA Journal*, vol. 47, pp. 331–344, 2009.